Applied Catalysis B: Environmental 339 (2023) 123137

Contents lists available at ScienceDirect

Applied Catalysis B: Environmental

journal homepage: www.elsevier.com/locate/apcatb

Photoinduced organocatalytic lignin C–C bond cleavage in mixed binary solvents

Yuting Liu [a,b], Huifang Liu [b,*], Ning Li [b], Feng Wang [a,b,**]

[a] Department of Chemical Physics, University of Science and Technology of China, Jinzhai Road 96, Hefei 230026, China
[b] Dalian Institute of Chemical Physics (DICP), Chinese Academy of Sciences (CAS), Dalian 116023, China

ARTICLE INFO

Keywords:
Lignin
Photocatalysis
C–C bond cleavage
Solvent effect

ABSTRACT

Lignin presents a renewable alternative of fossil feedstock to produce value-added aromatic chemicals. Oxidative cleavage of C−C bonds in lignin is of great importance, but obtaining aromatic monomers in high selectivity under mild conditions is challenging. Herein, we report a novel strategy of photoinduced oxidative C–C cleavage of lignin β–O–4 derivatives using photoredox organocatalysts, among which Mes-10-phenyl-Acr^{+}-BF_4^{-} exhibited high yields of aromatic aldehydes and phenyl formate. Besides, mixed binary organic solvents were demonstrated to promote bond cleavage and inhibit over-oxidation side reactions. The absorbance, excitation, and interaction with the lignin model of the photocatalyst in different solvents were investigated by UV-Vis, PL, and CV tests. Furthermore, through mechanism studies, a C-centered radical intermediate was captured, providing evidence for the direct $C_\alpha-C_\beta$ bond cleavage mechanism during the reaction. This work presents a new photocatalytic strategy and provides deep insights into the bond cleavage mechanism for lignin valorization.

1. Introduction

Lignocellulose is unique renewable organic carbon resource with great potential to replace fossil resources for the production of high-value chemicals, especially organic oxygenates [1–4]. Among them, lignin is the most abundant aromatic polymer in nature which accounts for approximately 25–35 % of the organic matrix of wood and lignocellulosic biomass [5–7]. Lignin has a rich aromatic cross-linked structure consisting of three simple phenylpropyl subunits that are functionally linked randomly by several different C−C and C−O bonds. The complex 3D cross-links and the diversity of bonding types confer rigidity and resistance to microbial and chemical degradation in woody plants [8,9]. The most common connection is β-O-4 linkage in lignin, which accounts for about 43–65% of all connection structures [10]. Efficient and selective cleavage of C−C/C−O bonds while retaining the aromatic ring structure is the key to produce high-value aromatic chemicals from lignin through catalytic depolymerization.

Traditional homogeneous and heterogeneous catalysis has been extensively studied for lignocellulose conversion, and the most widely used strategies include pyrolysis [11], gasification [12], acid or alkali-catalysis [13,14] and hydrogenolysis [15], with some processes already developed into commercial-scale technologies. Thermal catalysis generally requires high temperature to overcome the activation energy barrier. For example, catalytic lignin pyrolysis [16] is mostly performed at temperatures higher than 300 °C and hydrogenolysis [17] at temperatures higher than 150 °C. Heating is usually non-selective, so the selective activation of a specific functional group or chemical bond in the reactant is challenging to achieve. In general, reductive catalytic fractionation of lignin can generate monomers such as phenols, ketones, benzene or toluene, and these monomers can be further hydrogenated into cycloalkanes. Catalytic oxidation of lignin can produce more platform oxygenates or valuable products such as aromatic aldehydes, acids, or esters [18].

In recent decades, several promising photoredox catalytic lignin depolymerization methods have been developed by Mariano [19–21], Stephenson [22–25], Moody [26], Soo [27,28], Zhang [29], Hu [30] et al. Although these methods present varied strategies toward lignin transformation utilizing metal/organic photocatalysis under mild conditions [31,32], challenges and disadvantages still exist, such as the photoinduced oxidation process consumes stoichiometric bases or oxidants, which brings some environmental concerns [33,34], and the oxidation process requires multi-step redox transformation via

* Corresponding author.
** Corresponding author at: Dalian Institute of Chemical Physics (DICP), Chinese Academy of Sciences (CAS), Dalian 116023, China.
E-mail addresses: liuhuifang@dicp.ac.cn (H. Liu), wangfeng@dicp.ac.cn (F. Wang).

https://doi.org/10.1016/j.apcatb.2023.123137
Received 24 April 2023; Received in revised form 22 June 2023; Accepted 28 July 2023
Available online 29 July 2023

Table 1
Photoinduced reaction of 2-phenoxy-1-phenylethanol under different conditions [a].

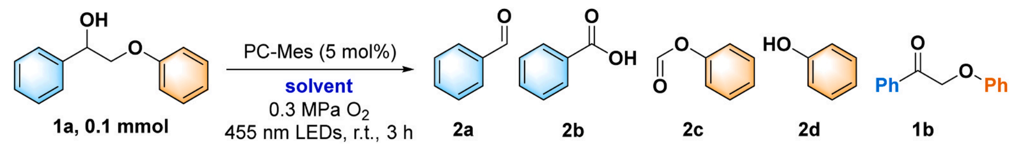

Entry	Solvent	Conv. (%)	Product Yield (%)				
			2a	2b	2c	2d	1b
1	Cyclohexane	6	5	0	4	0	0
2	THF	18	10	2	6	2	6
3	$CHCl_3$	83	69	4	58	2	0
4	CH_2Cl_2	100	2	78	49	4	0
5	DCE	100	2	78	54	3	0
6	Acetone	97	7	47	21	0	6
7	MeCN	100	11	32	16	1	0
8	DMF	6	0	0	0	0	3
9	DMSO	0	0	0	0	0	0
10	MeCN + $CHCl_3$	100	54	38	79	2	2
11[b]	MeCN + $CHCl_3$	93	55	20	64	2	8
12[c]	MeCN + $CHCl_3$	63	6	8	9	12	33
13[d]	MeCN + $CHCl_3$	27	0	0	0	14	11
14[e]	MeCN + $CHCl_3$	5	2	0	2	0	0

[a]Reaction conditions: substrate (0.1 mmol), PC-Mes (0.005 mmol), 455 nm LEDs, solvent (1.0 mL) or MeCN + $CHCl_3$ (v/v = 0.5: 0.5 mL) at room temperature (r.t.) for 3 h under 0.3 MPa of O_2. Overall yields were determined by GC with *n*-dodecane as an internal standard. PC-Mes = Mes-10-phenyl-Acr^+-BF_4^-. [b]Under 0.1 MPa of O_2. [c]Under Air. [d]Under Ar. [e]No PC-Mes.

photo/metal relay catalysis [35,36]. Most recently, we have studied the direct photocatalytic lignin depolymerization systems at room temperature using C_3N_4 semiconductor [37] and vanadium-based photocatalysts [38] without any additives, which demonstrate the main route of $C_\alpha-C_\beta$ bond cleavage in lignin β-O-4 linkages. However, there are still problems in the photocatalytic lignin valorization process, such as poor contact between solid catalysts and lignin matrix, slow redox cycle of active metal centers, and over-oxidization of the obtained phenolic derivatives.

At present, organic photocatalysis has developed into a powerful and diverse tool for catalysis research due to its tunable redox potential and high catalytic activity [39,40]. A wide variety of organic photocatalysts are used in combination with photoredox catalysis modes. Therefore, we sought to address these issues by developing a mild and controllable method for oxidative lignin depolymerization, which can modulate the active radical species [41], realize selective cleavage of C–C bonds, and increase the overall yield. Herein, we present a protocol of photoinduced oxidative $C_\alpha-C_\beta$ bond cleavage of lignin β-O-4 derivatives using metal-free photosensitizers as the catalyst, which can obtain high value-added aldehydes and formates in high yields. And mixed solvents were found to promote the substrate conversion and inhibit some over-oxidation processes, which reveals synergistic effects in the photoredox catalysis.

2. Experimental

2.1. Materials

All solvents and reagents purchased from commercial suppliers were of analytical-reagent grade, and were directly used for the reaction without further purification. Some lignin β-O-4 derivatives were synthesized on the basis of referring to relevant information.

2.2. Photocatalytic reactions

Typical photocatalytic reactions were carried out in a customized quartz tube (6 mL) under 455 ± 5 nm LED light with a total power of 11 W. Typically, 0.1 mmol of a lignin model, 0.005 mmol of the photocatalyst and 1 mL of solvent were firstly added into the reactor. And the oxygen gas was charged to 0.3 MPa, after which the tube was sealed and placed under LED light illumination, the reaction mixture was stirred for a desired time. *CAUTIOUS! Wearing eye goggle of shielding 455 nm light is mandatory*. After reaction, *n*-dodecane as an analytical internal standard was added into the reaction mixture. The liquid sample was diluted and analyzed by gas chromatography-mass spectrometry (GC-MS) and gas chromatography (GC). Conditions of gas chromatography: Agilent 7890B, DB-FFAP column; nitrogen carrier gas; split injection; injector temperature: 220 °C; temperature program: firstly maintaining 60 °C for 3 min, then increasing to 220 °C by 10 °C/min, finally maintaining 220 °C for 15 min

The conversion and yield were calculated in molar percent as follows:

$$\text{Conversion}(\%) = \left(1 - \frac{n(\text{substrate unreacted})}{n_0(\text{substrate})}\right) \times 100\%$$

$$\text{Yield}(\%) = \frac{n(\text{target} \quad \text{product})}{n_0(\text{substrate})} \times 100\%$$

n_0(substrate) is the initial mole of substrate added.

n(target product) is the moles of the corresponding target product.

2.3. Analytical procedure

UV-vis absorption spectra in solution were recorded on a SHIMADZU UV-2600 UV/Vis spectrometer. Steady-state fluorescence emission spectra were performed on PTI-QM400 fluorescence spectrometer. Nuclear magnetic resonance (^{1}H NMR) spectra of compounds were measured on a Bruker AVANCE III HD 700 MHz. Electron paramagnetic resonance (EPR) spectra were taken on a Bruker spectrometer in the X-band at 293 K with a field modulation of 100 kHz. The microwave frequency was maintained at 9.3 GHz. The prepared solutions of indicated components were taken out into a small capillary tube under oxygen for EPR examination.

A Metrohm Autolab PGSTAT 302 N was used for the electrochemical measurements in a conventional three-electrode electrochemical cell installed with glassy carbon as the working electrode, platinum foil as the counter electrode, and 0.01 M Ag/$AgNO_3$ electrode as the reference electrode. Cyclic voltammetry (CV) curves were measured in 0.1 M Bu_4NPF_6 solution (degassed and moisture-free) and 0.05 mmol of substrate at a scan rate of 100 mV/s. All electrochemical measurements

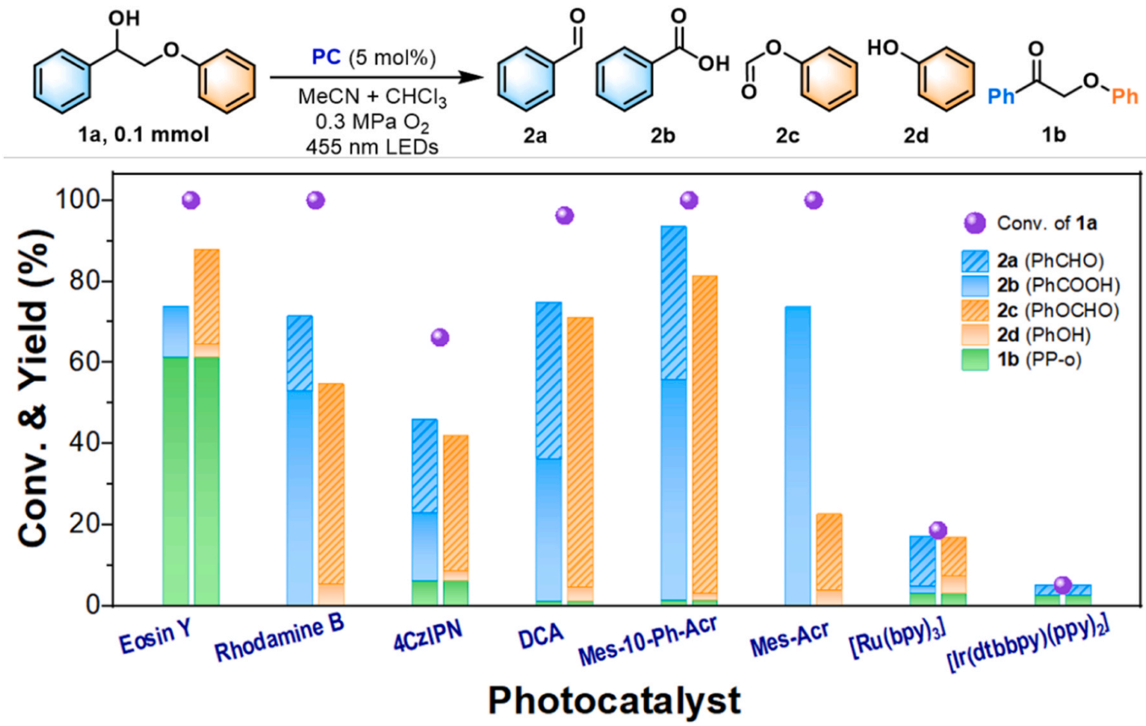

Fig. 1. Photocatalytic reaction of β-O-4 model (**1a**) with various photocatalysts. Reaction conditions: substrate **1a** (0.1 mmol), photocatalyst (0.005 mmol), 455 nm LEDs, solvent of MeCN + $CHCl_3$ (v/v = 0.5: 0.5 mL), r.t., 3 h, 0.3 MPa of O_2.

were performed at 25 °C. The potential for Ag/$AgNO_3$ nonaqueous reference electrode was 0.3 V versus SCE.

3. Results and discussions

3.1. Photocatalytic reaction of lignin model

Based on the literature and our previous work [42] on the understanding of oxidative lignin depolymerization, aromatic aldehydes, acids and phenols can be obtained after reaction of lignin models or native lignin. In this work, the oxidative reaction of lignin model, 2-phenoxy-1-phenylethanol (PP-ol, 1a), using Mes-10-phenyl-Acr^+-BF_4^- (PC-Mes) catalyst was selected as a prototypical system. A thorough evaluation of reaction conditions, including the solvents, photocatalysts,

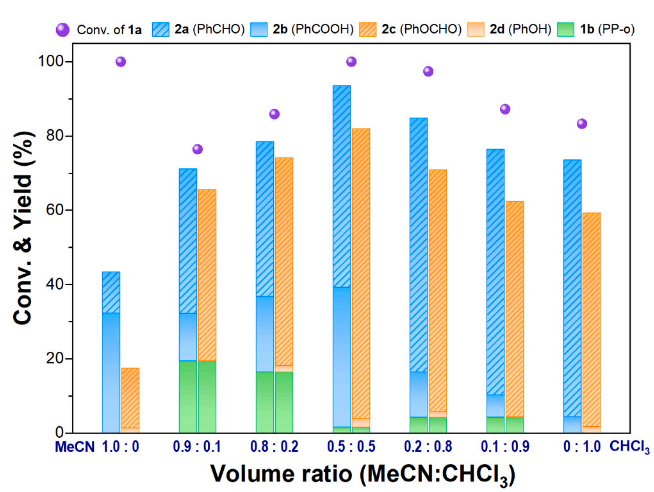

Fig. 2. Effects of mixed solvent ratio on the reaction of **1a**. Conditions: substrate **1a** (0.1 mmol), PC-Mes (0.005 mmol), 455 nm LEDs, solvent (1.0 mL), r.t., 3 h, 0.3 MPa of O_2.

and atmospheres were carried out, with the results summarized in Table 1.

Solvent type has great influence on the photocatalytic reaction. The oxidative reaction carried out in a single organic solvent such as cyclohexane or tetrahydrofuran (THF) showed a very low conversion of **1a** and product yields (Table 1, entries 1–2). When using chlorine-containing organic solvents such as $CHCl_3$, CH_2Cl_2 (DCM) or $C_2H_4Cl_2$ (DCE), the yields of monomer products increased to nearly 80% (entries 3–5). And the conversion of **1a** in $CHCl_3$ was slightly lower than that in CH_2Cl_2 or DCE, but the overall selectivity of monomer products in $CHCl_3$ was higher. In addition, the lignin model **1a** was almost completely converted in the acetone or acetonitrile (MeCN) solvent (entry 6 and 7), but the overall yield of the target products benzaldehyde (**2a**), benzoic acid (**2b**), phenyl formate (**2c**) and phenol (**2d**) was low, indicating that the selectivity of C–C bond cleavage was poor due to excessive side reactions in the system. In polar solvents such as DMF or DMSO (entry 8 and 9), the conversion of **1a** was very low, which could be due to the cage effect of solvent with larger viscosity that it severely hinders radical escape from the cage and decreases the quantum yield [43,44]. Moreover, the mixed solvent of MeCN and chloroform showed exciting effects (entry 10), that is, the product yield was significantly improved, in which the total yield of benzaldehyde (**2a**) and benzoic acid (**2b**) reached 92%, and the yield of phenyl formate (**2c**) increased to 79%. Control experiments (Table 1, entries 11–14) show that the reaction was a photocatalytic and aerobic oxidation process, and the increase of O_2 pressure promoted the reaction. Meanwhile, in the argon environment (entry 13), products produced from the C_β–O bond cleavage (acetophenone, phenol) were detected in the reaction system besides the oxidation product of 2-phenoxy-1-phenylethanone (PP-o, **1b**) (see Supporting Information, Fig. S2).

The reaction activities of different kinds of organic photocatalysts were further investigated. As shown in Fig. 1, when the common metal-organic photocatalyst such as $[Ru(bpy)_3]Cl_2$ or $[Ir(dtbbpy)(ppy)_2]PF_6$ was used [45], the conversion of β-O-4 model **1a** was less than 20% with a small amount of products obtained, mainly due to the low oxidation potentials ($E_{1/2}$(*Ru^{II}/Ru^{I}) = 0.77 V and $E_{1/2}$(*Ir^{III}/Ir^{II}) = 0.66 V vs.

Solvent	Dielectric constant
Hexane	2
1,4-dioxane	2.2
$CHCl_3$	4.8
THF	7.5
$HCOOCH_3$	8.5
CH_2Cl_2	9.1
DCE	10.4
^{i}PrOH	18
Acetone	21
MeOH	33
MeCN	37
DMF	38
DMSO	47

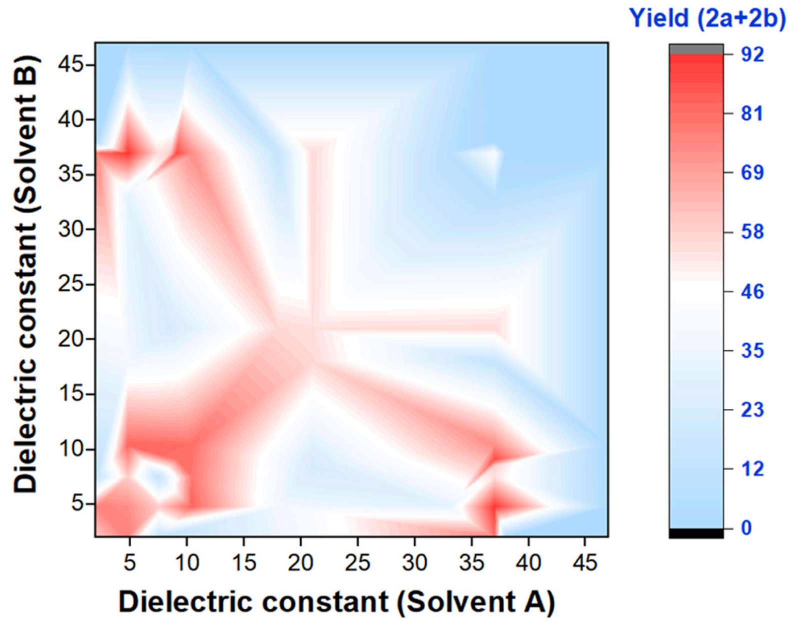

Fig. 3. Effects of various mixed solvents on the PC-Mes photocatalyzed reaction of **1a**. Conditions: substrate **1a** (0.1 mmol), PC-Mes (0.005 mmol), 455 nm LEDs, solvent (1.0 mL), r.t., 3 h, 0.3 MPa of O_2.

SCE, respectively) of the ground state of these two photocatalysts. When the dye photosensitizer Eosin Y ($E_{red}^{T1} = 0.83$ V) was used as the catalyst, the substrate **1a** was completely converted, but the main product was keto-product (**1b**) via the C_α–OH oxidation. Using Rhodamine B ($E_{red}^{S1} =$ 1.26 V) as the catalyst, the substrate **1a** was almost completely transformed with benzoic acid (**2b**) and phenyl formate (**2c**) as the main products, but the overall carbon yields still need to be improved, while 4CzIPN ($E_{red}^{S1} = 1.35$ V) photocatalyst showed much lower reactivity with a 66% conversion of **1a**. Besides, 9,10-anthracenedicarbonitrile (DCA) ($E_{red}^{S1} = 1.99$ V) as the photocatalyst increased the yield of phenyl formate (**2c**) to 70%. In comparison, the Mes-Acr^{+*} is a robust oxidant and has an excited state reduction potential of E_{red}^{S1} $= \sim 2.1 - 2.2$ V, thus when employing Mes-10-phenyl-Acr^{+}-BF_4^- as the catalyst, the highest yields of C−C cleavage products were obtained [46].

3.2. Solvent effect and oxidation potential of PC-Mes

Based on the results above, the mixed solvent containing MeCN and chloroform improved the product yield. The solvent ratio was further studied. As shown in Fig. 2, reaction of model **1a** was fast and the conversion reached 100% in the pure MeCN solvent after 3 h, but the target monomer yields were low (< 45%). When the proportion of MeCN was reduced to 0, that is, using the single $CHCl_3$ solvent, no **1b** was detected after reaction, indicating a high selectivity of C–C bond cleavage but the conversion was reduced to 83%. As the ratio of MeCN decreases and $CHCl_3$ increases in the mixed solvent, the conversion of **1a** and the overall product yield generally follow a volcano plot and the optimum system is V_{MeCN} /$V_{chloroform}$ = 0.5: 0.5, with the highest product yields achieved when V_{MeCN} /$V_{chloroform}$ reached 1:1.

The influence of other solvents in the mixed systems was further explored, while After determining that the optimal ratio of mixed solvents was 1:1, we further explored on the photocatalytic reaction of model **1a** in detail (as shown in Fig. 3). Together with the experimental results in Table 1, when the solvent with low dielectric constant (cyclohexane, THF) is mixed with another solvent with higher dielectric constant (DCM, DCE, MeCN), the conversion and product yields were both significantly improved compared with that in either of the single solvent. The product yield in the mixed solvent containing MeCN and the chlorine-containing solvent is significantly higher than that in a single solvent. Besides, the selectivity of C–C bond cleavage products was higher in the solvent mixture with chlorine-containing solvents (DCM, DCE, $CHCl_3$) is present in the system. However, in the systems containing solvent with high polarity and dielectric constant (MeOH, DMF or DMSO), whether mixed or not, the conversion and product yield were still very low. Therefore, the photocatalytic reaction path and activity can be optimized through the regulation of mixed solvent systems, and then the selectivity of C–C bond cleavage products can be improved.

The reactivity difference between the single solvent and the mixed solvent system is reflected in the difference of the ground state reduction potential ($E_{1/2}^{red}$) and excited state energy ($E_{0,0}^{S1}$) of the PC-Mes. From the CV analysis in Fig. 4b, the $E_{1/2}^{red}$ of PC-Mes was the smallest in single $CHCl_3$ solvent, and the largest in MeCN. The $E_{1/2}^{red}$ in the mixed solvents fell in the $E_{1/2}^{red}$ range between $CHCl_3$ and MeCN. It indicated the synergistic effect of photocatalyst and solvent in the reaction. In addition, the $E_{0,0}^{S1}$ of PC-Mes was almost the same among different solvents (Fig. 4c-e), according to the analysis of photoexcitation and potential value in Fig. 4a and f. Therefore, the excited state oxidation potential (E_{red}^{S1}) of PC-Mes catalyst was moderate (E_{red}^{S1} = 2.20V) in the mixed solvent, which means that it may have good catalytic activity for substrate conversion without excessive oxidation of certain products or intermediates.

3.3. Reaction mechanism

Then, the path and mechanism of the photocatalytic reaction were further studied. First, the time-relationship of substrate conversion and product formation was investigated (Fig. 5A), and it was found that with the decrease of substrate, the production of phenyl formate (**2c**) and benzaldehyde (**2a**) first increased synchronously, and then part of benzaldehyde was further converted to benzoic acid (**2b**), and phenol (**2d**) was kept at trace amount. The **1b** by-product increased slightly and then decreased, which may act as a minor pathway to obtain the cleavage product after further bond fragmentation.

In addition, comparing the reaction rate of **1b** with the substrate **1a**, it was found that **1b** could also undergo oxidative cleavage reaction to obtain benzoic acid and phenyl formate, and the reaction rate was faster

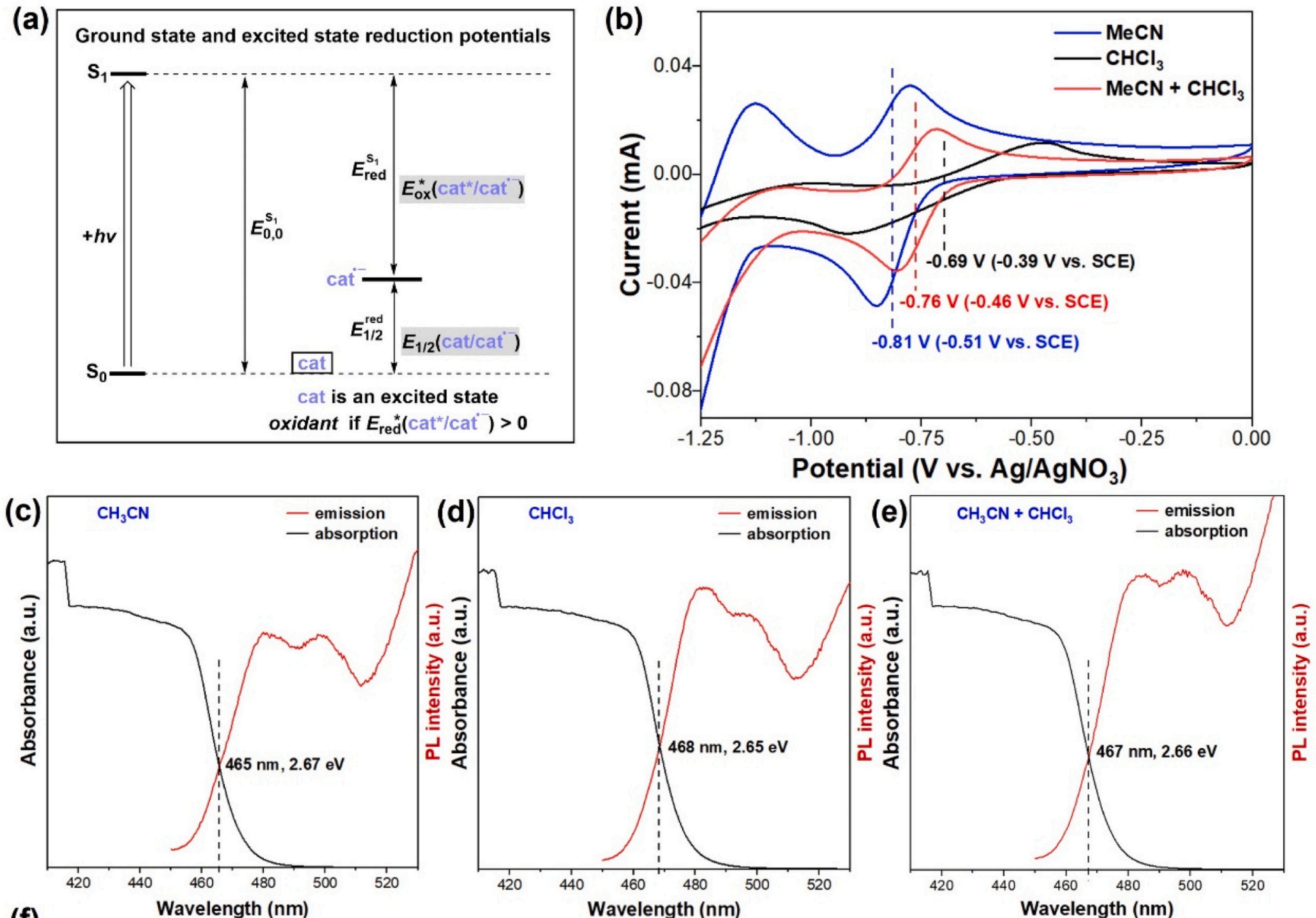

(f)

Solvent	excited state energies (eV) $E_{0,0}^{S1}$	ground state redox potentials (V vs SCE) $E_{1/2}^{red}$	excited state redox potentials (V vs SCE) E_{red}^{S1}
MeCN	2.67	-0.51	2.16
MeCN + $CHCl_3$	2.66	-0.46	2.20
$CHCl_3$	2.65	-0.39	2.26

Fig. 4. (a) Photophysical and electrochemical processes and properties of photoreduction catalysts. Copyright 2016, American Chemical Society. (b) Cyclic voltammograms of PC-Mes (2.5 mM) in a degassed solvent with 0.1 M Bu_4NPF_6 at a scan rate of 100 mV/s, a glassy carbon working electrode and with 0.01 M Ag/$AgNO_3$ as the reference electrode (0.3 V vs SCE). (c-e) UV-Vis absorption (black line) and emission spectra ($\lambda_{ex} = 440$ nm, red line) of PC-Mes (1.0 mM) in MeCN, $CHCl_3$ and in MeCN + $CHCl_3$, respectively. ($E_{0,0}^{S1} = \frac{1240}{\lambda}$, with λ at the intersection of absorption and emission spectra [47]) (f) Photophysical properties of the PC-Mes in different solvents. ($E_{red}^{S1} = E_{0,0}^{S1} + E_{1/2}^{red}$).

than that of **1a** (Fig. 5B and Fig. S6). However, a large amount of benzaldehyde is generated after reaction of **1a**, but benzoic acid is directly generated after the bond fragmentation of **1b** without any benzaldehyde, hence there may be two paths in the photocatalytic reaction system. The main path is that the substrate **1a** is directly oxidized to benzaldehyde and phenyl formate, and another path is that part of **1a** was oxidized to **1b** and then rapidly oxidized to corresponding benzoic acid and phenyl formate. Control experiments (Figs. 5B, (2−4)) show that benzaldehyde can be further oxidized to benzoic acid, phenyl formate may be converted to phenol in a small part, and phenol may be over-oxidized to form other polymerization by-products (Fig. S7). However, once the substrate was completely transformed in this system, main products of benzaldehyde, benzoic acid and phenyl formate were still stable. The side reactions were significant, resulting in a high overall product yield which further confirms the related reaction path.

During the radical trapping experiment, TEMPO (Fig. 5C) or BHT (Supporting Information, page S8) was added as a free radical inhibitor. TEMPO almost completely inhibited the oxidative cleavage reaction, indicating that the reaction was primarily a free radical process. Besides, we compared radical trapping experiments with different deuterated substrates **1a-*D***, and the C_β radical of alkyl ether was captured by TEMPO and detected by GC-MS ($m/z = 263$ for the adduct, for details, see Supporting Information, pages S9-S10), indicating that the intermediate was formed via C_α−C_β bond cleavage. Meanwhile, the C-centered radical intermediate was detected by electron paramagnetic resonance (EPR) with DMPO as a spin-trapping reagent during the reaction (Fig. 6d). The calculated hyperfine splittings are g_0 (2.0064), α_N (14.8 G) and α_H (21.1 G), which indicates the presence of C-centered radical intermediate during the transformation under light irradiation [48]. To gain insight into the rate-determining step for this oxidative depolymerization, kinetic isotopic effect (KIE) studies with **1a, 1a-α-*d*$_1$** and **1a-β-*d*$_2$** were carried out. The parallel KIE afforded the oxidation conversion and gave the k_H/k_D values of 0.98 and 0.90, respectively, and the intermolecular competition experiments gave the k_H/k_D values of 1.1 and 1.0, respectively (Fig. 5D). These results indicated that C−H bond cleavage is not the rate-determining step.

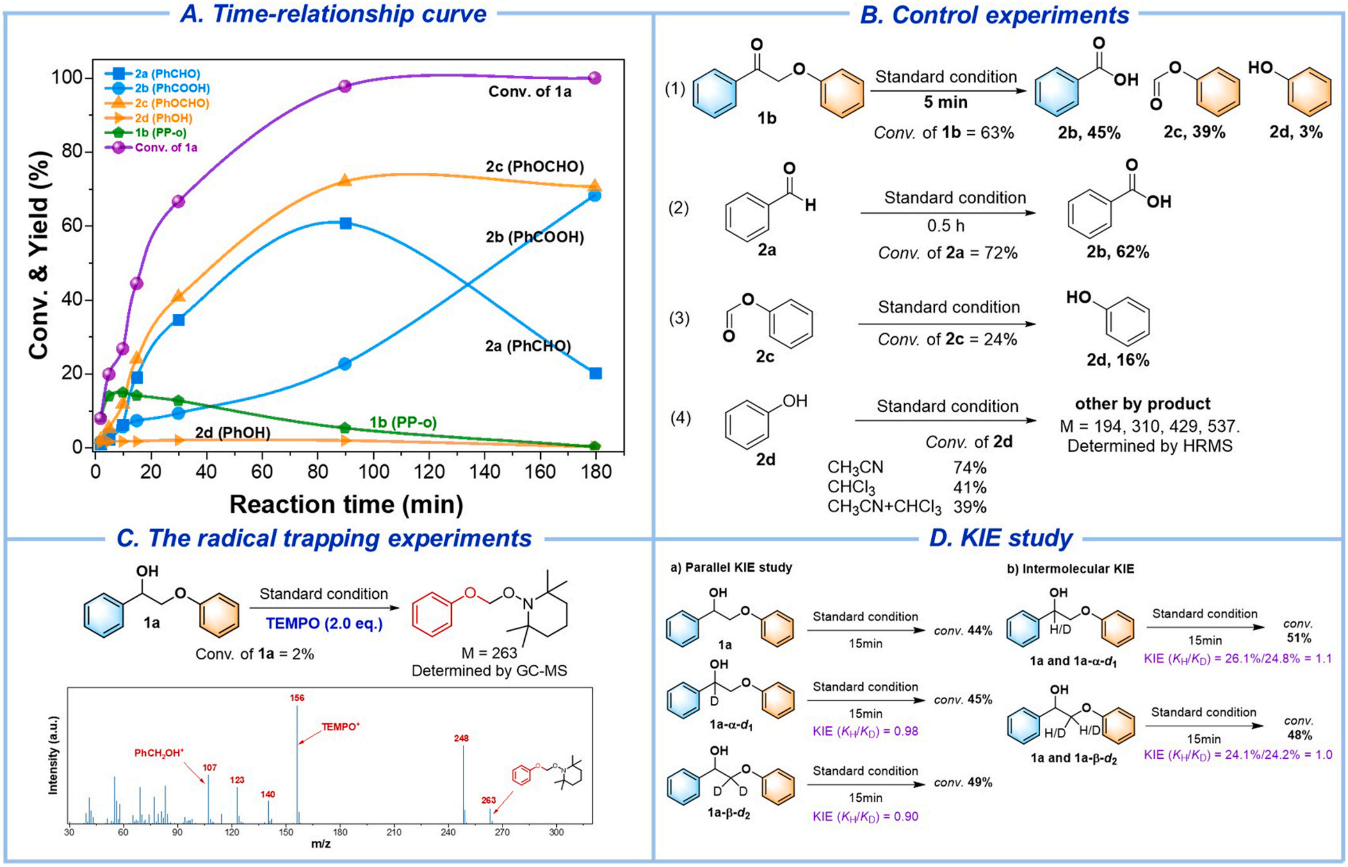

Fig. 5. Reaction path and mechanism studies. (A) The time relationship curve of **1a**. (B) Control experiments. Standard conditions: substrate (0.1 mmol) and PC-Mes (0.005 mmol) were irradiated using 455 nm LEDs in MeCN + $CHCl_3$ (v/v = 0.5: 0.5 mL) at r.t. under 0.3 MPa of O_2. (C) The radical trapping experiments (for details, see Supporting Information, page S8). (D) KIE study (for details, see Supporting Information, pages S11-S12).

We propose that the oxidative process was initiated by the photocatalyst excitation under blue light irradiation. Stern-Volmer quenching studies indicated a highly efficient quenching of the excited S_1-state of PC-Mes by the substrate ($k_q = (4.5 \pm 0.1) \times 10^9$ M^{-1} s^{-1}) (Fig. 6a-b) [49]. The hypothesis is fully consistent with the UV-Vis spectroscopic analysis (Fig. 6c). The PC-Mes showed absorption features at 455 nm to generate PC-Mes* . And the photocatalyst itself does not change much during the illumination (see Supporting Information, Fig. S8). Meanwhile, through comparing the UV-Vis spectroscopy of the reaction mixture before and after irradiation, with the increase of irradiation time, the absorption peak of the photocatalyst decreased, indicating that the substrate **1a** interacted with the excited photocatalyst. Simultaneously, the oxygen bubbles were injected into the system, absorption signals of the UV-Vis spectra decreased slightly compared with the initial state, which confirmed the cyclic regeneration process of the photoredox catalysis in the presence of oxygen.

Based on the above studies, the main path and reaction mechanism of oxidative lignin catalyzed by organic photocatalyst was proposed (Scheme 1). The process begins with the excitation of photocatalyst after blue light irradiation, and the excited state has strong oxidation capacity. Electron transfer occurs between the substrate **1a** and the organic photosensitizer (PC-Mes), with the substrate losing an electron and forming an **A-B** resonant intermediate. Keeping binding with $O_2^{\bullet-}$, the intermediate would form an alkoxy radical via hydrogen abstraction and induce $C_\alpha-C_\beta$ bond fragmentation to provide the product of benzaldehyde (**2a**) and the $\bullet C_\beta H_2OPh$ radical [50]. Then the intermediates continue to be oxidized and finally benzoic acid (**2b**) and benzyl formate (**2c**) were obtained.

3.4. Reaction of other lignin models

With the optimal conditions established, the scope of the reaction with respect to other readily available lignin models were investigated (Table 2). The β-O-4-**1b** was oxidatively transformed quickly and mainly obtained 90% benzoic acid under the same conditions after 0.5 h reaction. The multi-substitution β-O-4 model **1c** was also applicable to this method and can obtain the corresponding target products of aromatic acids and esters. It is worth noting that the Polymer-lignin-A-**1d** can be also smoothly transformed and obtain the desired target products such as benzaldehyde (40 %), benzoic acid (51 %), and phenyl formate (72 %). Therefore, this reaction system can effectively break C–C bonds of lignin β-O-4 derivatives and has the potential to be applied to real lignin.

4. Conclusions

In summary, we have developed a novel strategy of photoinduced oxidative C–C cleavage of lignin β-O-4 derivatives using photoredox organocatalysts, with high yields of aromatic aldehydes and phenyl formate obtained in mixed binary solvents. The photophysical properties of photocatalyst in different solvent systems were studied. The E_{red}^{S1} of PC-Mes catalyst was moderate (E_{red}^{S1} = 2.20V) in the mixed solvent, which can promote the substrate conversion and inhibit excessive oxidation of certain products or intermediates. Through the mechanism studies, a C-centered radical intermediate was captured, which proved that the $C_\alpha-C_\beta$ bond was cleaved in the reaction process, generating the free radical intermediate, and the following oxidative transformation occurred to obtain final products. Moreover, this reaction system is also

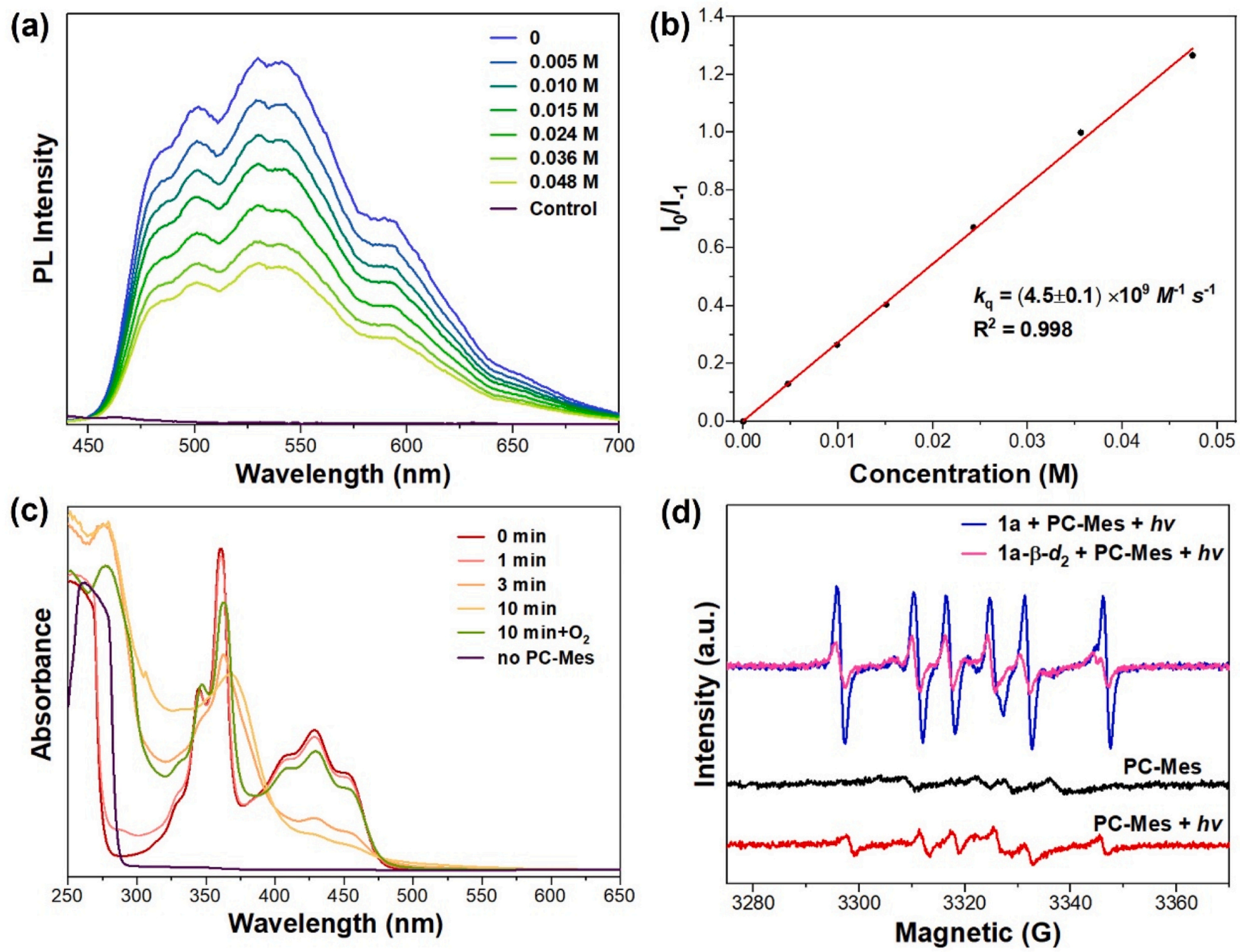

Fig. 6. Spectroscopic studies. (a) Fluorescence quenching of 0.1 mM PC-Mes by **1a**. (b) Stern-Volmer plot. (**c**) UV-Vis absorption spectra for the mixture of **1a** (0.1 mmol) and PC-Mes (0.005 mmol) in MeCN and $CHCl_3$ (v/v = 10: 10 mL) under Ar atmosphere. (d) EPR spectra obtained from the reaction mixtures: **1a** or **1a-β-d_2** (0.1 mmol), PC-Mes (0.005 mmol) and 5,5-dimethyl-1-pyrroline-*N*-oxide (DMPO, 0.1 mmol) in MeCN and $CHCl_3$ (v/v = 0.5: 0.5 mL).

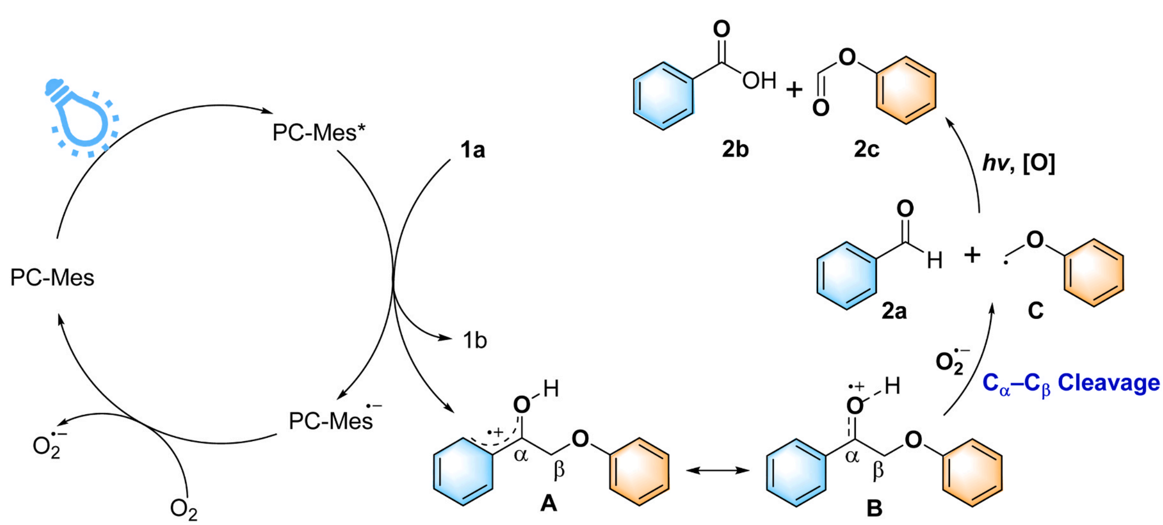

Scheme 1. Proposed mechanism in the photocatalytic cleavage of *β*–O–4 model by PC-Mes.

Table 2
Photocatalytic oxidative C−C cleavage of lignin *β*-O-4 model derivatives [a].

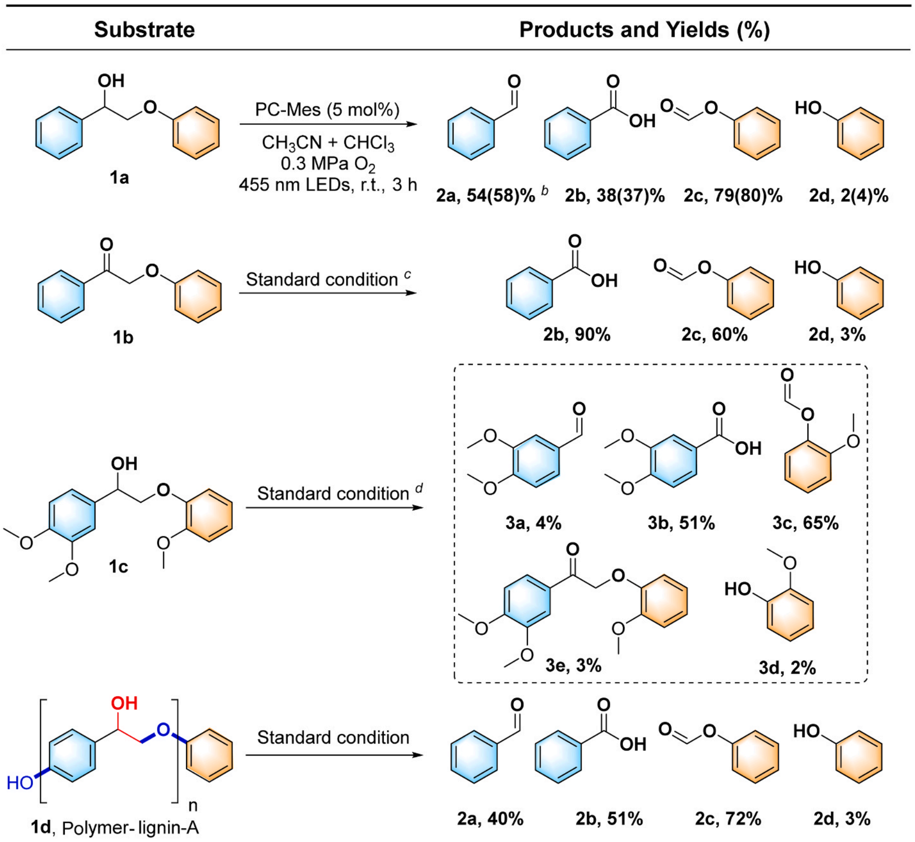

[a] Reaction conditions: Substrate (0.1 mmol) and PC-Mes (5 mol%) were irradiated using 455 nm LEDs in MeCN + $CHCl_3$ (v/v = 0.5: 0.5 mL) at r.t. for 3 h under 0.3 MPa O_2. PC-Mes = Mes-10-phenyl-Acr$^+$-BF4$^-$. [b] The yields in parentheses are using 2.5 mol% PC-Mes. [c] 1 mol% PC-Mes for 0.5 h. [d] **1c** (0.05 mmol).

suitable for oxidative C−C bond cleavage of various lignin *β*-O-4 derivatives.

CRediT authorship contribution statement

Y. Liu: Conceptualization, Methodology, Software, Data curation, Writing- Original draft preparation **N. Li**: Writing - review & editing, Software, Validation. **H. Liu**: Supervision, Writing - review & editing, Formal analysis **F. Wang**: Supervision, Writing - review & editing.

Declaration of Competing Interest

The authors declare that they have no known competing financial interests or personal relationships that could have appeared to influence the work reported in this paper.

Data Availability

Data will be made available on request.

Acknowledgements

This work was supported by the National Key R&D Program of China (2022YFA1504904), the National Natural Science Foundation of China (22272169, 22025206, 32130073), the Liaoning Revitalization Talents Program (XLYC2002012), the Dalian Institute of Chemical Physics, CAS (Grant: DICP I202131), and K. C. Wong Education Foundation of Chinese Academy of Sciences (GJTD-2020-08). We thank the instrumental support of the Liaoning Key Laboratory of Biomass Conversion for Energy and Material.

Appendix A. Supporting information

Supplementary data associated with this article can be found in the online version at doi:10.1016/j.apcatb.2023.123137.

References

[1] J. Zakzeski, P.C. Bruijnincx, A.L. Jongerius, B.M. Weckhuysen, The catalytic valorization of lignin for the production of renewable chemicals, Chem. Rev. 110 (2010) 3552–3599, https://doi.org/10.1021/cr900354u.
[2] C. Li, X. Zhao, A. Wang, G.W. Huber, T. Zhang, Catalytic transformation of lignin for the production of chemicals and fuels, Chem. Rev. 115 (2015) 11559–11624, https://doi.org/10.1021/acs.chemrev.5b00155.
[3] S. Gazi, Valorization of wood biomass-lignin via selective bond scission: a minireview, Appl. Catal. B: Environ. 257 (2019), 117936, https://doi.org/10.1016/j.apcatb.2019.117936.
[4] R. Ma, Y. Xu, X. Zhang, Catalytic oxidation of biorefinery lignin to value-added chemicals to support sustainable biofuel production, ChemSusChem 8 (2015) 24–51, https://doi.org/10.1002/cssc.201402503.
[5] K.V. Sarkanen, C.H. Ludwig, Liguins, Occur. Form. Struct. React. (1971).
[6] W.G. Glasser, R.A. Northey, T.P. Schultz, Lignin: historical, biological, and materials perspectives, ACS Publications1999.
[7] B. Saake, R. Lehnen, Lignin, Ullmann's. Encycl. Ind. Chem. (2000).
[8] W. Schutyser, T. Renders, S. Van den Bosch, S.F. Koelewijn, G.T. Beckham, B. F. Sels, Chemicals from lignin: an interplay of lignocellulose fractionation, depolymerisation, and upgrading, Chem. Soc. Rev. 47 (2018) 852–908, https://doi.org/10.1039/c7cs00566k.

[9] X.J. Shen, J.L. Wen, Q.Q. Mei, X. Chen, D. Sun, T.Q. Yuan, R.C. Sun, Facile fractionation of lignocelluloses by biomass-derived deep eutectic solvent (DES) pretreatment for cellulose enzymatic hydrolysis and lignin valorization, Green. Chem. 21 (2019) 275–283, https://doi.org/10.1039/c8gc03064b.

[10] C. Zhang, F. Wang, Catalytic lignin depolymerization to aromatic chemicals, Acc. Chem. Res. 53 (2020) 470–484, https://doi.org/10.1021/acs.accounts.9b00573.

[11] H. Kawamoto, Lignin pyrolysis reactions, J. Wood Sci. 63 (2017) 117–132, https://doi.org/10.1007/s10086-016-1606-z.

[12] A. Castro Garcia, S. Cheng, J.S. Cross, Lignin gasification: current and future viability, Energies 15 (2022) 9062, https://doi.org/10.3390/en15239062.

[13] S.-C. Qi, J.-i Hayashi, S. Kudo, L. Zhang, Catalytic hydrogenolysis of kraft lignin to monomers at high yield in alkaline water, Green. Chem. 19 (2017) 2636–2645, https://doi.org/10.1039/C7GC01121K.

[14] Z. Wu, L. Hu, Y.T. Jiang, X.Y. Wang, J.X. Xu, Q.F. Wang, S.F. Jiang, Recent advances in the acid-catalyzed conversion of lignin, Biomass. Conv. Bioref. 13 (2023) 519–539, https://doi.org/10.1007/s13399-020-00976-8.

[15] M. Zaheer, R. Kempe, Catalytic hydrogenolysis of aryl ethers: a key step in lignin valorization to valuable chemicals, ACS Catal. 5 (2015) 1675–1684, https://doi.org/10.1021/cs501498f.

[16] M. Asmadi, H. Kawamoto, S. Saka, Gas-and solid/liquid-phase reactions during pyrolysis of softwood and hardwood lignins, J. Anal. Appl. Pyrolysis 92 (2011) 417–425, https://doi.org/10.1016/j.jaap.2011.08.003.

[17] M.A. Hossain, T.K. Phung, M.S. Rahaman, S. Tulaphol, J.B. Jasinski, N. Sathitsuksanoh, Catalytic cleavage of the β-O-4 aryl ether bonds of lignin model compounds by Ru/C catalyst, Appl. Catal. A: Gen. 582 (2019), 117100, https://doi.org/10.1016/j.apcata.2019.05.034.

[18] M. Wang, F. Wang, Catalytic scissoring of lignin into aryl monomers, e1901866, Adv. Mater. 31 (2019), https://doi.org/10.1002/adma.201901866.

[19] D.W. Cho, R. Parthasarathi, A.S. Pimentel, G.D. Maestas, H.J. Park, U.C. Yoon, D. Dunaway-Mariano, S. Gnanakaran, P. Langan, P.S. Mariano, Nature and kinetic analysis of carbon–carbon bond fragmentation reactions of cation radicals derived from SET-oxidation of lignin model compounds, J. Org. Chem. 75 (2010) 6549–6562, https://doi.org/10.1021/jo1012509.

[20] D.W. Cho, J.A. Latham, H.J. Park, U.C. Yoon, P. Langan, D. Dunaway-Mariano, P. S. Mariano, Regioselectivity of enzymatic and photochemical single electron transfer promoted carbon-carbon bond fragmentation reactions of tetrameric lignin model compounds, J. Org. Chem. 76 (2011) 2840–2852, https://doi.org/10.1021/jo200253v.

[21] S.H. Lim, H. Jang, M.J. Kim, K.R. Wee, D.H. Lim, Y.I. Kim, D.W. Cho, Visible-light-induced selective C–C bond cleavage reactions of dimeric β-O-4 and β-1 lignin model substrates utilizing amine-functionalized fullerene, J. Org. Chem. 87 (2022) 2289–2300, https://doi.org/10.1021/acs.joc.1c01991.

[22] J.D. Nguyen, B.S. Matsuura, C.R. Stephenson, A photochemical strategy for lignin degradation at room temperature, J. Am. Chem. Soc. 136 (2014) 1218–1221, https://doi.org/10.1021/ja4113462.

[23] I. Bosque, G. Magallanes, M. Rigoulet, M.D. Karkas, C.R.J. Stephenson, Redox catalysis facilitates lignin depolymerization, ACS Cent. Sci. 3 (2017) 621–628, https://doi.org/10.1021/acscentsci.7b00140.

[24] C. Yang, M.D. Karkas, G. Magallanes, K. Chan, C.R.J. Stephenson, Organocatalytic approach to photochemical lignin fragmentation, Org. Lett. 22 (2020) 8082–8085, https://doi.org/10.1021/acs.orglett.0c03029.

[25] G. Magallanes, M.D. Kärkäs, I. Bosque, S. Lee, S. Maldonado, C.R.J. Stephenson, Selective C–O bond cleavage of lignin systems and polymers enabled by sequential palladium-catalyzed aerobic oxidation and visible-light photoredox catalysis, ACS Catal. 9 (2019) 2252–2260, https://doi.org/10.1021/acscatal.8b04172.

[26] L.J. Mitchell, C.J. Moody, Solar photochemical oxidation of alcohols using catalytic hydroquinone and copper nanoparticles under oxygen: oxidative cleavage of lignin models, J. Org. Chem. 79 (2014) 11091–11100, https://doi.org/10.1021/jo5020917.

[27] S. Gazi, W.K. Hung Ng, R. Ganguly, A.M. Putra Moeljadi, H. Hirao, H.S. Soo, Selective photocatalytic C–C bond cleavage under ambient conditions with earth abundant vanadium complexes, Chem. Sci. 6 (2015) 7130–7142, https://doi.org/10.1039/c5sc02923f.

[28] S. Gazi, M. Đokić, A.M.P. Moeljadi, R. Ganguly, H. Hirao, H.S. Soo, Kinetics and DFT studies of photoredox carbon–carbon bond cleavage reactions by molecular vanadium catalysts under ambient conditions, ACS Catal. 7 (2017) 4682–4691, https://doi.org/10.1021/acscatal.7b01036.

[29] Y. Wang, J. He, Y. Zhang, $CeCl_3$-promoted simultaneous photocatalytic cleavage and amination of C_α–C_β bond in lignin model compounds and native lignin, CCS Chem. 2 (2020) 107–117, https://doi.org/10.31635/ccschem.020.201900076.

[30] P. Li, R. Liu, Z. Zhao, F. Niu, K. Hu, Lignin C–C bond cleavage induced by consecutive two-photon excitation of a metal-free photocatalyst, Chem. Commun. 59 (2023) 1777–1780, https://doi.org/10.1039/d2cc06730g.

[31] Z.Y. Xiang, W.Y. Han, J. Deng, W.B. Zhu, Y. Zhang, H.L. Wang, Photocatalytic conversion of lignin into chemicals and fuels, ChemSusChem 13 (2020) 4199–4213, https://doi.org/10.1002/cssc.202000601.

[32] X. Wu, N. Luo, S. Xie, H. Zhang, Q. Zhang, F. Wang, Y. Wang, Photocatalytic transformations of lignocellulosic biomass into chemicals, Chem. Soc. Rev. 49 (2020) 6198–6223, https://doi.org/10.1039/d0cs00314j.

[33] Y. Wang, Y. Liu, J. He, Y. Zhang, Redox-neutral photocatalytic strategy for selective C–C bond cleavage of lignin and lignin models via PCET process, Sci. Bull. 64 (2019) 1658–1666, https://doi.org/10.1016/j.scib.2019.09.003.

[34] M. Zheng, Y. Huang, L.W. Zhan, J. Hou, B.D. Li, Visible-light-induced C–C bond cleavage of lignin model compounds with cyanobenziodoxolone, Tetrahedron Lett. 61 (2020), 152420, https://doi.org/10.1016/j.tetlet.2020.152420.

[35] M.D. Karkas, I. Bosque, B.S. Matsuura, C.R. Stephenson, Photocatalytic oxidation of lignin model systems by merging visible-light photoredox and palladium catalysis, Org. Lett. 18 (2016) 5166–5169, https://doi.org/10.1021/acs.orglett.6b02651.

[36] W. Zhou, J. Nakahashi, T. Miura, M. Murakami, Light/Copper relay for aerobic fragmentation of lignin model compounds, Asian J. Org. Chem. 7 (2018) 2431–2434, https://doi.org/10.1002/ajoc.201800520.

[37] H. Liu, H. Li, J. Lu, S. Zeng, M. Wang, N. Luo, S. Xu, F. Wang, Photocatalytic cleavage of C–C bond in lignin models under visible light on mesoporous graphitic carbon nitride through π–π stacking interaction, ACS Catal. 8 (2018) 4761–4771, https://doi.org/10.1021/acscatal.8b00022.

[38] H. Liu, H. Li, N. Luo, F. Wang, Visible-light-induced oxidative lignin C–C bond cleavage to aldehydes using vanadium catalysts, ACS Catal. 10 (2020) 632–643, https://doi.org/10.1021/acscatal.9b03768.

[39] T. Bortolato, S. Cuadros, G. Simionato, L. Dell'Amico, The advent and development of organophotoredox catalysis, Chem. Commun. 58 (2022) 1263–1283, https://doi.org/10.1039/d1cc05850a.

[40] D. Ravelli, M. Fagnoni, A. Albini, Photoorganocatalysis. What for? Chem. Soc. Rev. 42 (2013) 97–113, https://doi.org/10.1039/c2cs35250h.

[41] Z.P. Huang, N.C. Luo, C.F. Zhang, F. Wang, Radical generation and fate control for photocatalytic biomass conversion, Nat. Rev. Chem. 6 (2022) 197–214, https://doi.org/10.1038/s41570-022-00359-9.

[42] C. Zhang, F. Wang, Sell a dummy: adjacent functional group modification strategy for the catalytic cleavage of lignin β–O–4 linkage, Chin. J. Catal. 38 (2017) 1102–1107, https://doi.org/10.1016/s1872-2067(17)62858-4.

[43] J. Franck, E. Rabinowitsch, Some remarks about free radicals and the photochemistry of solutions, Trans. Faraday Soc. 30 (1934), https://doi.org/10.1039/TF9343000120.

[44] R. Noyes, Tests of solution models by quantum yields for dissociation, Z. Electrochem. (1960), https://doi.org/10.1002/bbpc.19600640151.

[45] J.I. Day, K. Teegardin, J. Weaver, J. Chan, Advances in photocatalysis: a microreview of visible light mediated ruthenium and iridium catalyzed organic transformations, Org. Process Res. Dev. 20 (2016) 1156–1163, https://doi.org/10.1021/acs.oprd.6b00101.

[46] N.A. Romero, D.A. Nicewicz, Organic photoredox catalysis, Chem. Rev. 116 (2016) 10075–10166, https://doi.org/10.1021/acs.chemrev.6b00057.

[47] A.C. Benniston, A. Harriman, P. Li, J.P. Rostron, H.J. van Ramesdonk, M. M. Groeneveld, H. Zhang, J.W. Verhoeven, Charge shift and triplet state formation in the 9-mesityl-10-methylacridinium cation, J. Am. Chem. Soc. 127 (2005) 16054–16064, https://doi.org/10.1021/ja052967e.

[48] J. Deng, C. Zhou, Y. Yang, B. Nan, L. Dong, L. Cai, L. Li, Z.-J. Wang, X. Yang, Z. Chen, Visible-light-driven selective cleavage of C–C bonds in lignin model substrates using carbon nitride-supported ruthenium single-atom catalyst, Chem. Eng. J. 462 (2023), 142282, https://doi.org/10.1016/j.cej.2023.142282.

[49] N.A. Romero, D.A. Nicewicz, Mechanistic insight into the photoredox catalysis of anti-markovnikov alkene hydrofunctionalization reactions, J. Am. Chem. Soc. 136 (2014) 17024–17035, https://doi.org/10.1021/ja506228u.

[50] H.G. Yayla, H. Wang, K.T. Tarantino, H.S. Orbe, R.R. Knowles, Catalytic ring-opening of cyclic alcohols enabled by PCET activation of strong O–H bonds, J. Am. Chem. Soc. 138 (2016) 10794–10797, https://doi.org/10.1021/jacs.6b06517.